

Reconfigurable Hydrostatics: Toward Multifunctional and Powerful Wearable Robotics

Jeff Denis¹, Frédéric Laberge¹, Jean-Sébastien Plante¹ and Alexandre Girard¹

Abstract—Wearable and locomotive robot designers face multiple challenges when choosing actuation. Traditional fully actuated designs using electric motors are multifunctional but oversized and inefficient for bearing conservative loads and for being backdrivable. Alternatively, quasi-passive and underactuated designs reduce the size of motorization and energy storage, but are often designed for specific tasks. Designers of versatile and stronger wearable robots will face these challenges unless future actuators become very torque-dense, backdrivable and efficient.

This paper explores a design paradigm for addressing this issue: reconfigurable hydrostatics. We show that a hydrostatic actuator can integrate a passive force mechanism and a sharing mechanism in the fluid domain and still be multifunctional. First, an analytical study compares how these two mechanisms can relax the motorization requirements in the context of a load-bearing exoskeleton. Then, the hydrostatic concept integrating these two mechanisms using hydraulic components is presented. A case study analysis shows the mass/efficiency/inertia benefits of the concept over a fully actuated one. Then, the feasibility of the concept is partially validated with a proof-of-concept that actuates the knees of an exoskeleton. The experiments show that it can track the vertical ground reaction force (GRF) profiles of walking, running, squatting, and jumping, and that the energy consumption is 6x lower. The transient force behaviors due to switching from one leg to the other are also analyzed along with some mitigation to improve them.

Index Terms—Hydraulic/Pneumatic Actuators, Legged Robots, Underactuated Robots, Static Load Compensation.

I. INTRODUCTION

Mobile robots that must bear their own weight have conflicting design requirements. For reasonable autonomy, their actuators should be lightweight and efficient, but at the same time they need good backdrivability for good physical interaction with their environment, e.g., with the ground for a legged robot or with the user for an exoskeleton; and still to be useful in various situations (multifunctional), they should have high strength and power levels.

The recent research in legged robots and exoskeletons push mainly for lightly geared electric motors for their high velocity and relatively good torque density and backdrivability [1]–[3]. These actuators 1) have low inertia for better interactions and simpler force control, 2) have high transmission efficiency, and 3) enable good energy regeneration at batteries [1], [4]. However, by producing high electromagnetic torque, their motors heat significantly. For instance, the running legged robot Cheetah could regenerate most of its negative power to the battery, but 74% of its energy consumption was due to motor heating [1]. Over lightly geared motors, for even

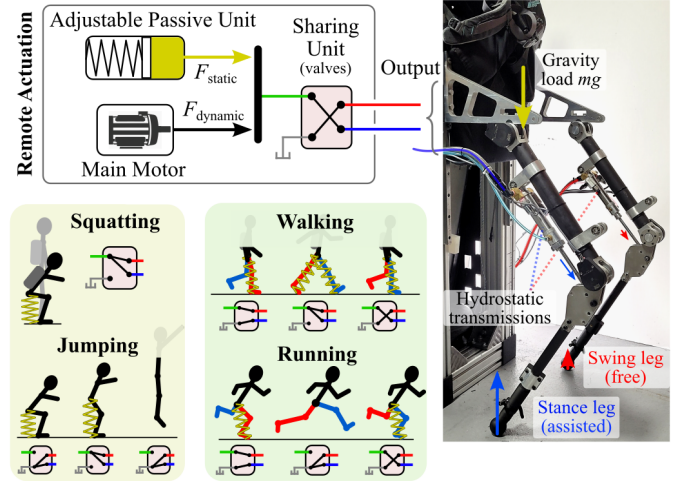


Fig. 1. Overview of the proposed multifunctional actuator. The same color coding is used through the paper for their corresponding variables and signals.

higher backdrivability, continuous slippage clutches like magnetorheological (MR) clutches were also proposed [5]. All these single-actuator-per-DOF (degree of freedom) strategies race for the highest force and power density actuator without compromising versatility.

To relax the motorization requirements of each DOF and improve efficiency, a passive element like a spring can be added, as in series-elastic and parallel-elastic actuators (SEAs, PEAs) [6]. Some exoskeletons are even passive only [7] [8] and do not need active motorization. However, these concepts are typically working for a specific task only.

To reduce the number of motors in multiple DOFs systems, the actuation may be shared as well. For instance, a hydraulic pump can distribute its power to many DOFs with servovalves and achieve highly dynamic and powerful tasks when this power is distributed to a few joints, like when the humanoid Atlas from Boston Dynamics jump [9]. This is multifunctional but typically results in high energy losses at the unused joints leading to a heavier centralized motor and energy storage. An alternate way to share actuation is underactuation, for instance exoskeletons that can fully disconnect the actuator from an unused joint to power another one, like for assisting the left and the right legs during stance [10]. However, so far, these concepts can only assist specific tasks.

As discussed above, quasi-passive actuators and sharing actuation were proposed as lighter/more efficient/cost effective solutions compared to fully actuated devices, but at the expense of low versatility. In a previous paper, the authors proposed to leverage hydrostatic transmissions to implement various hybrid actuation modes such as gravity-load compen-

¹All authors are with the Department of Mechanical Engineering, Université de Sherbrooke, Qc, Canada. (Corresponding author: jeff.denis@usherbrooke.ca.)

sation [11]. This paper describes, analyzes and tests a new reconfigurable hydrostatic topology that is multifunctional and combines both 1) an adjustable static force compensation, and 2) sharing the same actuation through multiple degrees of freedom. An overview is given in Fig. 1. The first contribution is the hydrostatic actuator topology that combines both two mechanical principles and still assist various exoskeleton tasks. The second contribution is an analysis showing how these units relax the motorization requirements for different tasks and how the total actuation mass, efficiency and inertia compares for a given case study. The third contribution is an experimental study of a load-bearing knee exoskeleton that can assist walking, running, squatting, and jumping, along with strategies to improve switching with valves.

Section II goes deeper into the state-of-the-art regarding passive load balancing and actuator sharing through multiple joints. Section III presents an analysis showing how these two principles can relax the motorization requirements. Section IV presents the proposed hydrostatic actuator and a case study analysis to compare the total mass, efficiency and inertia advantage with off-the-shelf components. Section V presents a proof-of-concept and a basic controller which is tested in section VI to validate experimentally that it can track the force profiles of walking, running, squatting and jumping and be more efficient as well. Finally, section VII presents control mitigation using the valves to improve the switching effects.

II. RELATED WORK

This section presents how the state-of-the-art locomotive robots and lower-limb exoskeletons applied static load compensation and actuator sharing, these two operating principles being integrated into the actuator of this paper. Although being promising for efficiently bearing payloads and for reducing the number of motors, most existing designs lack being multifunctional.

A. Efficient Static Load Compensation

Legged locomotion is an energy recycling process. For conservative force problems like walking/running at constant speed on flat ground, passive designs are more efficient and lighter than active designs using motors, but not as versatile. Fig. 2 shows how increasing the complexity of passive mechanisms can lead to more functionalities. First, a parallel grounded spring could bear a load without needing any energy, just like a car's suspension do. Quasi-passive exoskeletons often use this principle: a parallel spring fits the natural force-displacement behavior of a joint for the stance phase, as long as a clutching mechanism can disconnect the swinging leg [7] [8]. This approach shown by Fig. 2a is, however, typically task-specific since the ideal joint stiffness varies widely between tasks like squatting, walking and running.

Instead of matching the stiffness of a joint, a passive device can generate a constant force independent of the output motion, for static load compensation. One approach is to use static load compensation mechanisms, e.g., with counterweight mechanisms [12], but it increases significantly the weight and inertia, or with springs and non-linear transmissions (see

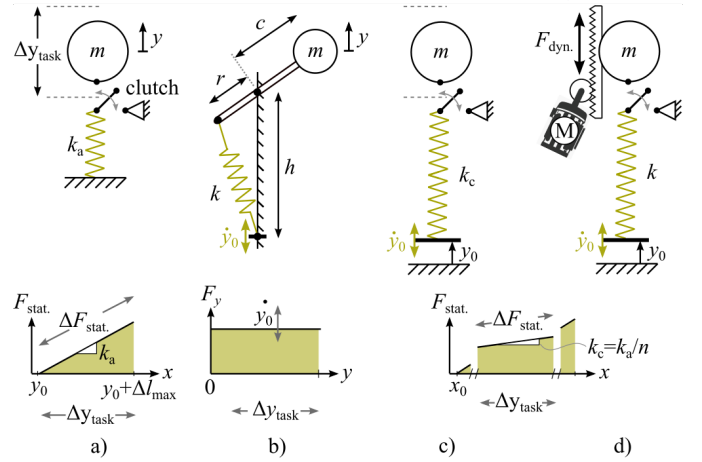


Fig. 2. Spring-based mechanisms in evolution of complexity and functionalities: a) clutchable spring, b) static balancing mechanism with adjustable attachment, c) a + large spring + adjustable y_0 , d) c + parallel actuator.

Fig. 2b), as done in [13] for balancing a human leg or in [14] for a robotic knee using a nitrogen gas spring and a non-linear cam mechanism. These concepts lack the flexibility to adjust the passive assistance on purpose which would make them more multifunctional.

To provide adjustable passive assistance, a first approach is to actively change the stiffness k of the spring similarly to variable stiffness actuators. Otherwise, the equations of the static force $F_{\text{stat.}}$ generated by the spring highlights other solutions. For the mechanism of Fig. 2b, it is $F_{\text{stat.}} = khr/c$. Therefore, one could move the attachment points of the spring to vary h and r . This was done by [15] for an efficient robotic leg using a small non-backdrivable actuator, but this collocated solution along the leg is rather complex to implement. For the concept of Fig. 2a, the force equation is $F_{\text{stat.}} = k(y - y_0)$. As k gets lower, the assistance becomes less dependent to the output motion y and acts similarly to a static balancing mechanism. Then, a low-power motor can move the spring attachment y_0 to change the passive assistance. The adjusting mechanism may be simpler to implement than for Fig. 2b but, as k gets lower, heavier springs and adjusting motors are needed.

Indeed, given the two concepts 2a and 2c with the same maximal force and assuming that 2c is n times more compliant ($k_{2c} = k_{2a}/n$), the maximum potential energies stored are $E_{2a} = k_a \Delta l_{2a, \text{max}}^2 / 2$ and $E_{2c} = k_{2c} \Delta l_{2c, \text{max}}^2 / 2 = nE_{2a}$. Thus, assuming that the mass of a spring m_k is proportional to its energy stored and that the mass of a highly geared motor m_{HGM} is proportional to its rated power $E/\Delta t$, we find $m_k \propto n$ and $m_{\text{HGM}} \propto n$. The feasibility of this solution depends on how strong and how compliant the spring has to be, how fast (Δt) the assistance shall be adjusted and how energy-dense and power-dense the spring and geared motors are, respectively.

So far, concepts 2a–c relied solely on a passive actuator force but for many applications, this is not sufficient. Indeed, dynamic force capabilities $F_{\text{dyn.}}$ are needed to move the legs of a legged robot and can benefit to exoskeletons to follow the

correct GRF force trajectories of different tasks and improve the transitions between the stance and the swing phases. In Fig. 2d, a parallel active actuator is added to the static load compensation system. This results in a parallel-elastic actuator but with a very compliant spring and an adjusting mechanism. A research robotic leg implements this principle in [16], [17] with a high-power series-elastic actuator that is coupled in parallel to a passive unit consisting of an elastic band being stretched by a non-backdrivable screw to balance a payload. A clutch can also actively disconnect the elastic band for the swing phase and for charging powerful jumps. The authors present a torque distribution control strategy and measured a 65% energy consumption reduction for squatting motions when using the passive unit. The concept was pushed further for monoarticular and biarticular 3-DOF leg designs in [18] with similar energy improvements for squats. Very recently, Fan et al. proposes a hydrostatic concept that works differently to carry payloads. Their hydrostatic support comprises a hydraulic cylinder per leg, a shared accumulator (acting as the spring) and switching valves for the swing phase. They leverage the fact that a robotic leg can be controlled during the stance phase of walking to make the height of the body still. The hydraulic cylinder provides a passive support but as it does not move during stance, the accumulator pressure does not vary and can be designed small [19]. However, this is not applicable for exoskeletons (the human body moves vertically) or for any tasks that need a vertical motion such as running (for smooth landing) and squatting.

So far, this concept is marginal in robotics and can be limited to assist specific tasks. Compensating heavy payloads such as human-scale robots with low energy-dense springs could be cumbersome, especially if collocated along the legs. Delocalization and using high energy density springs would benefit to this concept.

B. Actuator Sharing Through Multiple Joints

Most locomotion and wearable robots have one actuator per DOF. Fully actuated designs have controllability at all time, but can be overdesigned since torque requirements vary widely between tasks. For instance, during the stance phase, the human knee torque is relatively low for walking ($0.5\text{--}0.7 \text{ N m kg}^{-1}$) [20] compared to the torque for running ($3.0\text{--}4.0 \text{ N m kg}^{-1}$) [21]. Synergies in locomotion can be exploited to reduce the number of required actuators while keeping the possibility assisting many joints. The joints of the left and the right legs either work in-phase (e.g., squats, sit-to-stands and jumps), sharing the same force profiles, or out-of-phase (e.g., the stance phases of walking and running). Underactuation draw increasing attention in the recent years in lower-limb soft exosuits, with remote motorization in the back. In [22], with a differential gearbox, one motor can assist both hips during lifting motions, without hindering out-of-phase motions like walking. In [23], a second differential gearbox is added to power the lower-back joint as well, so three joints for a single motor. In [10], [24], a single motor assists the stance phases of walking of both hips thanks to the buckling effect of cable transmissions which decouple the motor from the swinging

leg. Other authors proposed multiarticular actuation like for the Myosuit which successfully reduces muscle efforts due to gravity loads by assisting simultaneously the knee and hip of one leg [25].

All current exoskeletons sharing the same actuation for the left and right legs have the same limitation: they can either assist in-phase or out-of-phase tasks but never both (at best, they just do not hinder it). Moreover, all existing designs rely on cable transmissions or differential gear mechanisms only. A multifunctional underactuated exoskeleton that shares actuation for both legs is yet to be developed.

In this section, it was stated that a static force passive unit and a sharing unit can benefit to a locomotive robotics. In the next section, we calculate how these two functions can actually relax the total motorization requirements in the context of a lower-limb exoskeleton.

III. EFFECT ON THE MOTORIZATION REQUIREMENTS

We discussed two mechanical principles that can potentially improve lightly geared actuator designs: 1) adding an adjustable static passive force unit and 2) adding a sharing unit. Here we assess how much these functions can relax the motorization requirements and improve efficiency of a load-bearing exoskeleton. It is found that when combining the two mechanical principles, the total RMS force to be generated by the main motors gets 2.7x to 7.8x lower.

Let's introduce a 2-DOF multitask exoskeleton that assists the vertical ground reaction forces (GRF_y) of the right leg f_1 and the left leg f_2 , for instance to reduce the musculoskeletal stress and the metabolic expenditure when carrying payloads like in [25] [26]. The following analysis is valid regardless of how these functions are mechanically obtained. Four generic designs are described by Fig. 3 and are compared in this section for four tasks: walking, running, jumping and sit-to-stands (similar to squatting). Note that Designs C and D could not work for a legged robot since they need motorization for the swing phase.

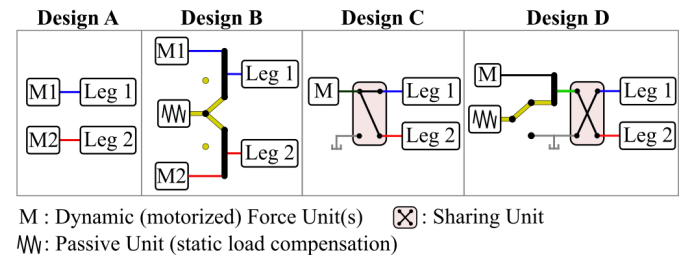


Fig. 3. The four generic designs compared in this analysis: A) fully actuated, B) with passive unit, C) with sharing unit, D) with both units.

Fig. 4 (first column) gives the typical normalized vertical GRF curves used, in N kg^{-1} or m s^{-2} of young human adults, obtained from papers and public datasets [20], [21], [27], [28].

A. Comparison Metrics

For long cyclic tasks like walking and running, the force output of an electric motor is most likely limited by its continuous rated torque. To prevent overheating, the continuous torque

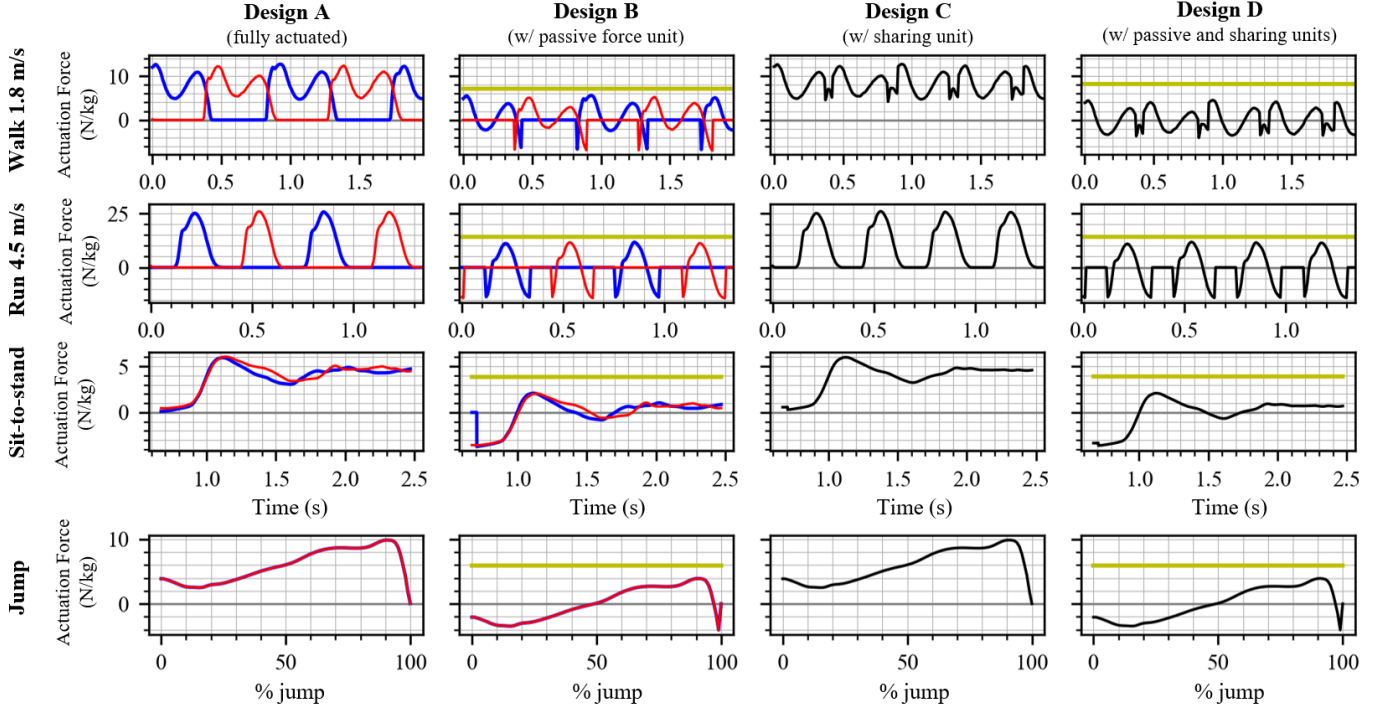


Fig. 4. Vertical GRF to be generated by the actuation for walking, jumping, sit-to-stand and jumping for the generic designs A–D (blue, red and black lines are the dynamic force for the right, left or for both legs, respectively, and yellow line for the static force offset when applicable).

of a motor should be higher than the RMS torque required for the task. The RMS torque also indicates how much energy is lost by heating because it is proportional to the winding current I , $\overline{P}_{\text{Joule}} = R \overline{(I(t)^2)} = RI_{\text{rms}}^2$. Recall that Joule's losses are often the main source of energy consumption for lightly geared motors [1]. Then, the RMS force metric $f_{\text{dyn,rms}}$ should be minimized for lightweight motorization and battery pack. Another relevant metric for power consumption in cyclic tasks is the mean absolute power $\overline{|P_{\text{dyn}}(t)|}$ generated by the dynamic force unit. Indeed, some mechanical output power is lost during both power generation $P_{\text{dyn}}^+(t)$ and regeneration $P_{\text{dyn}}^-(t)$. The total battery power is then given by equation 1 where $\eta_{\text{gen.}}$ and $\eta_{\text{regen.}}$ are the efficiency when generating and dissipating power, respectively. For energy conservative cyclic tasks, the mean positive and negative output powers cancel out, $\overline{P_{\text{dyn}}^+(t)} = -\overline{P_{\text{dyn}}^-(t)}$, giving equation 2.

$$P_{\text{battery}}(t) = P_{\text{Joules}}(t) + \frac{P_{\text{dyn}}^+(t)}{\eta_{\text{gen.}}} + \eta_{\text{regen.}} P_{\text{dyn}}^-(t) \quad (1)$$

$$\overline{P}_{\text{battery}}(t) = \overline{P}_{\text{Joules}}(t) + \left(\frac{1}{\eta_{\text{gen.}}} - \eta_{\text{regen.}} \right) \frac{\overline{|P_{\text{dyn}}(t)|}}{2} \quad (2)$$

Hereby, as $\overline{|P_{\text{dyn}}(t)|}$ gets lower, the energy consumption decreases. A lightly geared actuator with a bidirectional drive can regenerate to the battery most of the energy dissipated at the motor [1], but still there are transmission losses. Assuming $\eta = 90\%$, only 21% of the mechanical power is lost, whereas it is 73% for an inefficient highly geared transmission ($\eta = 70\%$). Another important metric is the peak force $f_{\text{dyn,peak}}$, especially for low duty cycle tasks like jumping and sit-to-stands where the motors do not have the time to heat. The

transmission sizing (e.g., gearbox) is also often based on this metric. Finally, for powerful tasks like jumping and running, the maximum speed $V_{\text{dyn.}}$ can also be limiting but increasing the supply voltage is a common mitigation.

B. Calculation

Here is described how the metrics are computed for Designs A–D and all the tasks. For Design A, the two motors should directly track the output force curves of each leg, meaning that for out-of-phase tasks (walking and running), each motor is used only 25-50% of the gaits. The RMS dynamic force of each leg i is:

$$f_{\text{A,dyn,rms},i} = \sqrt{\frac{1}{T} \int_0^T f_i(t)^2 dt} \quad (3)$$

For Design B, the passive unit offsets by a static force $f_{\text{stat.}}$ the dynamic force of each motor. We assume this passive force constant and that it does not consume energy once it is set for a given task and payload. An intuitive choice for $f_{\text{stat.}}$ is the gravity acceleration $g = 9.8 \text{ m s}^{-2}$. Actually, the mean value of the total GRF of each task is near g . However, this choice does not necessarily minimize the RMS force. The optimal static force offset that minimizes $f_{\text{dyn,rms}}$ is found by solving numerically equation 4:

$$f_{\text{B,stat},i}^* = \underset{f_{\text{B,stat},i}}{\operatorname{argmin}} \underbrace{\sqrt{\frac{1}{T} \int_0^T f_{\text{B,dyn},i}(t)^2 dt}}_{f_{\text{B,dyn,rms},i}} \quad (4)$$

subject to $f_{\text{B,dyn,rms},i} \leq \frac{\max |f_{\text{B,dyn},i}(t)|}{3}$

where:

$$f_{B,dyn,i}(t) = \begin{cases} f_i(t) - f_{B,stat,i} & \text{if } f_i(t) > 0 \\ 0 & \text{otherwise} \end{cases} \quad (5)$$

because when a leg is in the aerial phase, the static force unit is disconnected. The constraint limits the peak force needed at the motors to three times its continuous force as for typical electric motors [29].

For Design C, a single dynamic force unit is designed to track to total output force f_{out} :

$$f_{tot}(t) = f_1(t) + f_2(t) \quad (6)$$

We assume a differential-like mechanism for the transmission after the actuator when both legs are connected to the actuator. In this condition, the actuator speed and $V_{sharing}$ and force $f_{sharing}$ are:

$$V_{sharing}(t) = V_1(t) + V_2(t) \quad (7)$$

$$f_{sharing}(t) = f_1(t) = f_2(t) \quad (8)$$

From equations 6 and 8, the total GRF is doubled when the number of legs connected to the actuation N_{legs} is 2 which happens during walking, squatting and jumping. For any N_{legs} , the required dynamic force at the motor is given by:

$$f_{C,dyn}(t) = \begin{cases} \frac{f_1(t)+f_2(t)}{N_{legs}(t)}, & \text{if } N_{legs}(t) > 0 \\ 0, & \text{otherwise} \end{cases} \quad (9)$$

Finally, for Design D, the static force is found by solving equations 4 and 5, but replacing $f_i(t)$ by equation 9.

C. Results

Fig. 4 shows for each task the analytical force trajectories required at the motor(s) for Designs A–D, and the static force offset computed. From this, Table I gives the resulting metrics at the main motorization.

TABLE I
PERFORMANCE METRICS TO GENERATE BY THE MOTOR(S) (M) WHEN LEG(S) ARE ON GROUND FOR ALL TASKS AND DESIGNS

Design		A		B		C	D
		-		Passive		-	Passive
		-		-		Sharing	Sharing
Task	Metric*	M ₁	M ₂	M ₁	M ₂	M	M
Walk (1.8 m/s)	$f_{dyn,rms}$	6.5	6.5	2.3	2.3	8.6	2.4
	$f_{dyn,peak}$	13.4	13.4	7.0	7.0	13.7	5.5
	$ P_{dyn} $	0.47	0.47	0.14	0.14	0.93	0.22
	V_{dyn}	0.4	0.4	0.4	0.4	0.7	0.7
Run (4.5 m/s)	$f_{dyn,rms}$	9.7	9.7	5.1	5.1	13.7	7.2
	$f_{dyn,peak}$	26.6	26.6	13.9	13.9	27.4	14.1
	$ P_{dyn} $	1.0	1.0	0.72	0.72	2.0	1.4
	V_{dyn}	1.0	1.0	1.0	1.0	1.0	1.0
Jump (0.4 m)	$f_{dyn,peak}$	9.9	9.9	4.1	4.1	9.9	4.1
	V_{dyn}	2.7	2.7	2.7	2.7	5.4	5.4
Sit-to-stand	$f_{dyn,peak}$	6.0	6.0	3.7	3.7	6.0	3.6
	V_{dyn}	0.7	0.7	0.7	0.7	1.4	1.4

*All metrics are normalized by the user's bodyweight, $f_{dyn,rms}$ and $f_{dyn,peak}$ in $N \text{ kg}^{-1}$, $|P_{dyn}|$ in $W \text{ kg}^{-1}$, with the exception of V_{dyn} in m s^{-1} .

First, regarding motor sizing, the motor designs are not limited by the peak force but rather by the RMS force (heating) for walking and running, assuming a motor can generate up to 3x its nominal torque. However, for jumping and sit-to-stand, the peak force is a better metric for motor sizing since these are non-repetitive tasks.

Relative to Design A, the **passive force offset** of Design B significantly reduce the motors and gearbox sizes. For instance, the RMS forces are down to 2.8x lower for walking and down to 1.8x lower for running. This also means a better efficiency with less motors heating and also less transmission losses (smaller $|P_{dyn}|$) if we assume that the transmission efficiency is the same for both designs.

In the case of **sharing** (Design C), when compared to Design A, it divides by two the total force of tasks with combined legs (sit-to-stand, jumping and for 15% of the walking cycle) but it needs twice the speed (and stroke). For combined legs tasks, the motorization size is thus halved if it is not limited by the speed. Similarly, the total gearbox/transmission size is halved since the total peak force of all tasks is halved. Regarding the total RMS force of walking and running, it is only $\approx 1.3x$ lower, though. Sharing needs just one motor, but a faster one and a bigger one to prevent overheating. The weight advantage is therefore not certain and depends on how the motors torque-to-inertia and power density vary with size. As for energy consumption, the same transmission losses are expected, but less total motor heating losses, so Design C is more efficient, especially because the motor constant (in $N \text{ m W}^{-2}$) increases with motor size [30].

Finally, when both principles are **combined** (Design D), the benefits of the passive force and sharing combines too. It results in a solution likely more efficient and lighter regarding the motorization and transmission of the dynamic force unit.

This analysis showed how sharing and adding a static load compensation contribute to improving efficiency and reduce the requirements of motorization for a load-bearing lower-limb exoskeleton. However, implementing these functions is not trivial and requires extra components that could lead to a heavier actuation system. The next section presents a novel design that implements for the first time both principles in a single device, along with a deeper case study comparison.

IV. RECONFIGURABLE HYDROSTATICS PROPOSITION AND CASE STUDY

So far this paper discussed the potential of sharing actuation and adjustable static load compensation for locomotive robots and exoskeletons. Here is proposed a design opportunity to leverage hydrostatic transmissions and hydraulic components to implement both functions. Then, the results from section III are used in a specific case study analysis showing that the new design can be more backdrivable and consumes 3.9x less power for the same performance and total actuation weight.

A. Proposed Design

Hydrostatic transmissions are an alternative to cable transmissions to remotely actuate leg joints, leading to low-inertia robotic legs/exoskeletons. As discussed in section II,

adjustable static load compensation was proposed previously for a robotic leg using elastic bands, a screw transmission and a clutch. A pump, an accumulator and a motorized valve can do the same functions in the hydraulic domain, and can be shared to multiple joints if using more valves as shown in Fig. 5a. Since it acts in parallel, the passive force unit does not impede

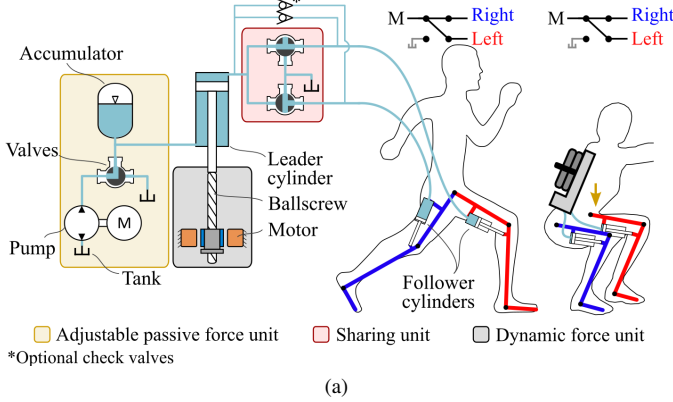


Fig. 5. Proposed actuator topologies for a lower-limb exoskeleton: a) for an adjustable passive force unit, b) for actuator sharing between the left and right joints, and c) for the combination of both principles into a single topology.

the force bandwidth of the main motor and may not increase significantly the backdriving force if designed properly. For sharing, the state-of-the-art exoskeletons rely on buckling cables or differential gearboxes to either assist in-phase or out-of-phase tasks, as discussed in section II. To assist both type of tasks, switching mechanisms like clutches would be needed. In the hydraulic domain, the hydrostatic transmissions can be a fluidic differential and switching is possible using valves. This way, three motors and three valve units could assist a multifunctional 6-DOF lower-limb exoskeleton. During the swing phase, the user backdrives the swinging leg being connected to the low-pressure tank. For in-phase tasks like squatting, the pressure is shared and the flow is split between the legs. Finally, in the hydraulic domain, both functions can be combined as shown in Fig. 5 for a knee exoskeleton. It is the design implemented experimentally in this paper. The authors believe that merging the two design principles is more complex when using clutches, brakes and gearboxes, instead of with hydraulic components like here. Still, the passive unit and sharing functions add extra components to the system. The following case study compares this concept to a fully actuated one by the selection of off-the-shelf components.

B. Case Study Comparison

Section III showed how a passive unit and a sharing unit can relax the requirements of lightly geared actuators for a load-bearing lower-limb exoskeleton. A deeper analysis using off-the-shelf components will now show the actual benefits of the proposed design regarding the total actuation mass, inertia and efficiency. Suppose a strong multifunctional 2-DOF exoskeleton for infantry that can unload significantly its user's bodyweight (up to 100% BW) when walking, allowing carrying heavy payloads. This exoskeleton could also assist

(or at least not restrain) running, jumping and squatting when needed. The requirements are:

- R1** User Bodyweight: 75 kg
- R2** Max 1.8 m/s Walking Assistance: 100% BW
- R3** Peak GRF Force (**R2** \times **R3**): 1000 N/leg (fig. 4)
- R4** Vertical Leg Stroke: 0.4 m
- R5** Work-per-Stroke (**R3** \times **R4**): 400 J/stroke/leg
- R6** Max Jumping Speed: 2.8 m/s

The RMS force motor requirements from Table I are used to design the dynamic force units. The whole transmission designs after the leader piston(s) are driven by **R5**. For speed, the jumping task is the most constraining one for the design, especially when sharing the same motor for both legs.

Fig. 6 illustrates the resulting Designs A and D along with their performance maps in Fig. 7 to show how much force assistance each design can provide for each task. For

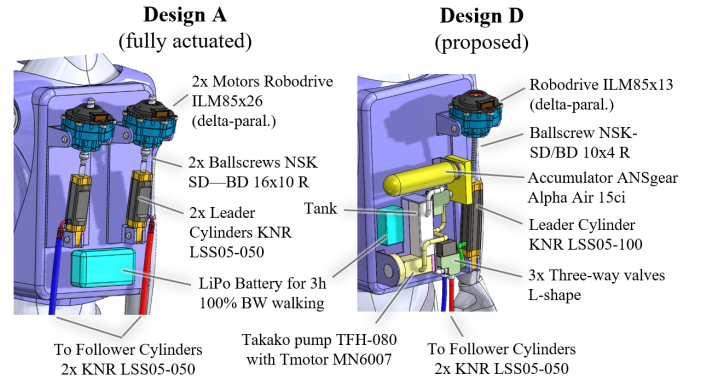


Fig. 6. Case study illustrative CAD. All actuation is located in the user back and actuates remotely the vertical GRF of the legs.

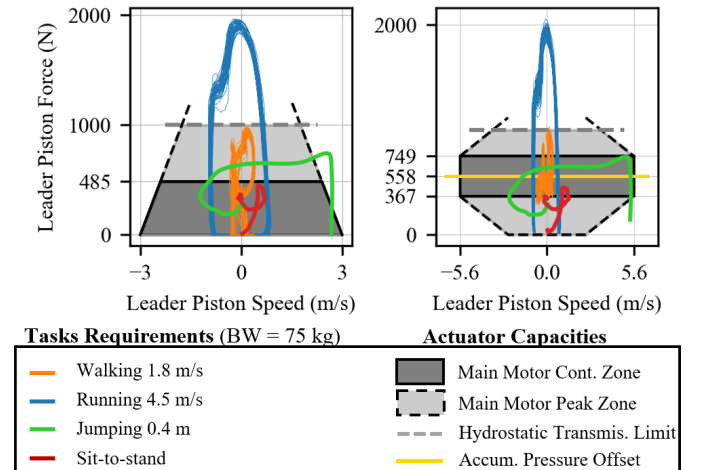


Fig. 7. Performance map coverage of the actuator designs from the case study, as seen in the vertical output reference frame. Both designs have enough speed to cover all tasks and each one can assist at a similar force amplitude a 75 kg BW user.

Design A, the total ratio between the dynamic force unit motors and the output is $R_{\text{motor-GRFy}} = 186 \text{ m}^{-1}$, whereas it is $R_{\text{motor-GRFy}} = 147 \text{ m}^{-1}$ for Design D. With similar performance, the designs can be compared with Table II regarding mass, efficiency and inertia. Even with the extra

components that Design D needs, the total mass is similar. The

TABLE II
CASE STUDY COMPARISON

Performance	Design A (fully actuated)	Design D (proposed)
Power Consumption (W)¹	77	20
Main motor(s) heat losses	62	16
Transmission losses	15	4
Mass w/o Battery (kg)	4.0	3.9
Frameless Motor(s)	1.34	0.40
Ballscrew(s)	1.24	0.12
Leader Cylinder(s)	0.98	0.65
Follower Cylinders	0.98	0.98
Fluid	0.07	0.31
Accumulator		0.22
Motorized pump		0.61
Valves		0.60
Battery mass per hour ² (kg/h)	0.50	0.07
Reflected Inertia at each Leg (kg)	3.8	1.4
Motor	3.66	1.32
Ballscrew (nut rotating)	0.15	0.10

¹ At nominal motor(s) torque, i.e. the RMS power for a 100%BW continuous walking assistance at 1.8 m/s. Transmissions losses assuming 90% ballscrew efficiency for both designs.

² For the given power consumption, assuming 150 W h kg⁻¹ LiPo batteries.

power consumption is 3.9x lower for Design D, which means more autonomy or a lighter battery pack. For Design A, we note that, as a reference, the same motors are used as in the backdrivable leg prosthesis of Elery et al. [3] but here driving instead two ball screws and two hydrostatic transmissions to actuate each leg remotely. The reflected inertia of Design A is thus equivalent to this state-of-the-art backdrivable prosthesis designed for walking. For Design D, the resulting inertia is 2.7x lower, increasing the backdrivability, especially for powerful tasks like running and jumping.

The actual mass/efficiency/inertia advantage of Design D over a fully actuated hydrostatic one varies with the requirements. Since it needs extra components, it will be more likely beneficial when a high force-to-inertia ratio is desired, e.g., for strong backdrivable robots. Also, a fully actuated design collocated near the knees, without hydrostatic transmissions, like in [3], would be globally lighter but more cumbersome with heavy components near the knees and still would be less efficient and backdrivable than Design D.

V. PROOF-OF-CONCEPT DESIGN AND CONTROL

This section presents the design of a proof-of-concept to validate the experimental feasibility of the proposed concept of Fig. 5. It also introduces the basic force control and switching control strategies for the validation.

A. Test Bench Design

The proof-of-concept is a knee exoskeleton driven by a remote power unit on a table, as shown by Fig. 8. Table III summarizes the specifications and the selected components.

TABLE III
PROOF-OF-CONCEPT COMPONENTS AND SPECIFICATIONS

Description	Var.	Value
System Specifications at Output for 1 Leg [2 legs]		
Max Vertical Force (N)	-	366 [711]
Max Dynamic force (N)	$F_{dyn,peak}$	81 [162]
Max Static Force (N)	$F_{stat.}$	366 [711]
No-load Speed (m s ⁻¹)	-	9.1 [4.6]
Reflected Inertia* (kg)	-	0.2 [0.4]
Exo. Single Leg Mass (kg)	-	3.0
Exo. Mass (Legs+Rail) (kg)	m_{proto}	13.4
Main Motor		Maxon RE50 (48V)
Torque constant (N m A ⁻¹)	K_T	0.093
Torque (N m)	-	0.42 cont. 1.4 peak
Ballscrew (BS)		NSK MCM05025H20K00
Lead (mm/turn)	L_{BS}	20
Screw diameter (mm)	-	12
Cylinders (L=leader, F=follower)		Bimba H-093-DUZ
Max pressure (MPa)	-	3.45
Piston Area (mm ²)	A	572
Piston Area (rod side) (mm ²)	A_r	524
Strokes	x_L x_F	203 76
Hydrostatic Transmission		SUM-230610
Internal Diameter (mm)		8.7 (-6 AN)
Length (mm)		1000
Fluid		Recochem 35-365WP
Accumulator		Stauff STDA-0500
Nominal (gas) volume (mL)	V_{a0}	500
Max pressure (MPa)	P_a	21
Precharge pressure (MPa)	P_{a0}	1.03
Max compression ratio	-	1:8
Gear Pump		0AM325579D
Fluid	-	Pentosin CHF 11S
Pressure-Speed slope (Pa.s)	m_p	9709
Motorized Valves		McMaster 4149T42
Max pressure (MPa)	-	10.3
Internal Diameter (mm)	-	6.35
Servomotor	-	AGFRC A80BHP-H
Stall Torque (N m)	-	1.8
0-180° switching speed (ms)	-	80
0-113° switching speed (ms)	-	60

*Including motor, screw and fluid transmission inertia.

1) *Exoskeleton and Transmission*: The knee exoskeleton is non-anthropomorphic and designed to assist the vertical GRF. The hip joints are free and the knee joints are actuated by the two follower pistons. By deriving the kinematic equations of the robotic leg, the positions of the piston rod attachments (lever mechanism) were computed to minimize the variation of vertical force assistance with respect to leg vertical stroke at a given pressure, as shown by the plot on the upright corner of Fig. 8. The prototype allows for different attachment configurations to change this output ratio on purpose. The configuration with maximum vertical stroke has an average ratio of the vertical rail force over the follower piston force of $\bar{R} = 0.18$. The leader piston has twice the stroke of the follower pistons for having full leg stroke when both legs are connected to it. The transmission fluid was chosen for its low viscosity at room temperature, low toxicity and anti-corrosion properties.

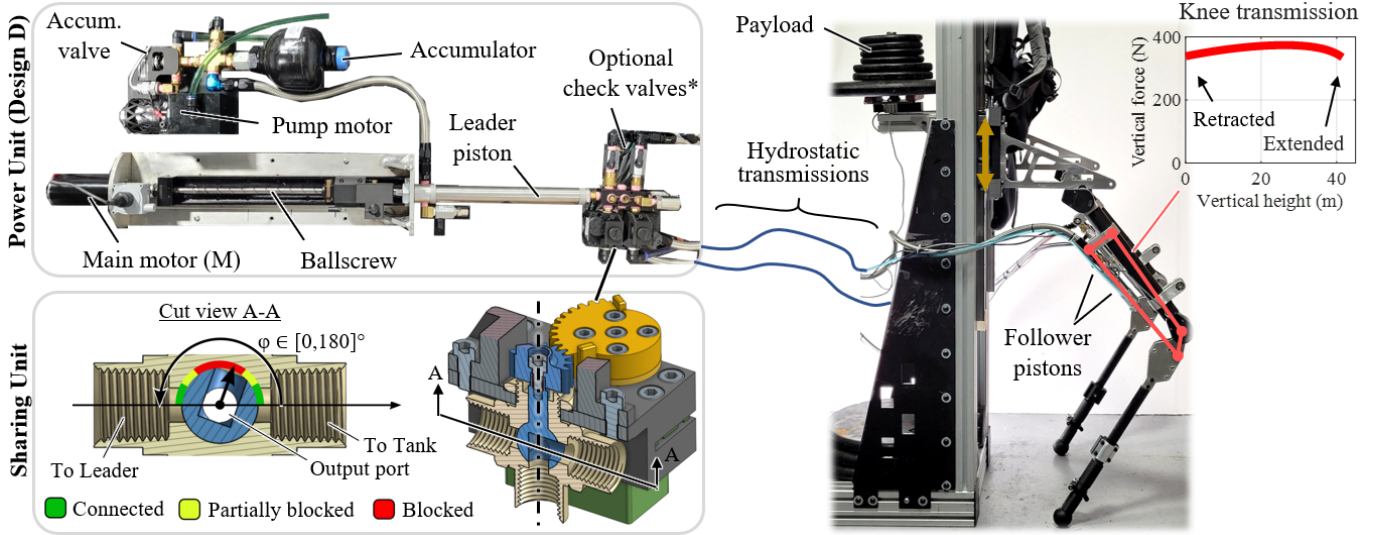


Fig. 8. Overview of the actuator proof-of-concept remotely powering the knees of an exoskeleton and its custom motorized ball valves.

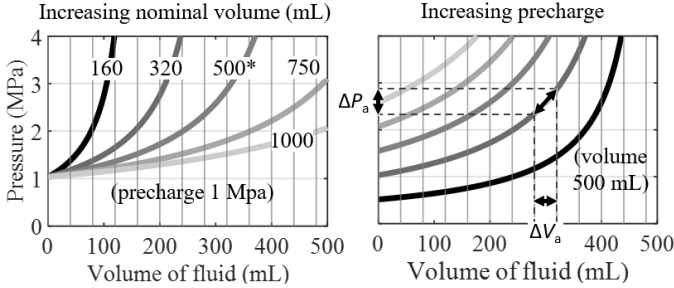


Fig. 9. Effects of the accumulator nominal (gas) volume and the gas precharge on the pressure-volume curves. *Curve of the accumulator used for the experimental setup.

2) *Adjustable Passive Force Unit*: Hydraulic accumulators have either a gas spring behavior (bladder and diaphragm accumulators) or a linear spring behavior (piston with a spring). A diaphragm accumulator is here selected for its low friction. For sizing the accumulator, two main factors influence its behavior: its nominal gas volume $V_{a,0}$ (size) and its gas precharge $P_{a,0}$. The perfect gas law gives the relationship between the accumulator pressure P_a and volume V_a :

$$P_a = P_{a,0} \frac{V_{a,0}^n}{(V_{a,0} - V_a)^n} \quad (10)$$

where $n = 1$ for isothermic change (slow) and $n = 1.4$ for adiabatic (fast) change and for nitrogen gas. Fig. 9 shows the effect of $V_{a,0}$ and $P_{a,0}$ on the pressure-volume relationship. We want the quasi-static output force assistance not to vary much with leg stroke. When the leader piston moves, V_a varies, inducing a variation of pressure ΔP_a as shown by Fig. 9. This effect can be reduced by: 1) using a high precharge $P_{a,0}$, but it decreases the available low-pressure range, 2) increasing the volume of the accumulator, but it increases its mass and the need for a powerful pump that fills it within a reasonable time, 3) designing the transmission at output to cancel out the effect of ΔP_a at output, but this would not be effective when changing the number of joints connected to the actuator,

or 4) increasing the overall system rated pressure because it decreases the displaced volume of the pistons (for the same work-per-stroke, less piston stroke or area is needed). The later point also means that the cylinders and accumulator are more compact for higher pressure rated systems. For the current setup, a 500 mL gas volume and a 1 MPa precharge is chosen. The pump is a small gear pump for car transmissions and can generate up to 3.5 MPa with the fluid suggested by the manufacturer. Its viscosity is higher than for the hydrostatic transmission but it has minor effects on backdrivability since this circuit is short.

3) *Dynamic Force Unit*: This unit is a lightly geared actuator that generates 0.77 MPa in the transmission, at peak torque. The ball screw has a high lead which makes it backdrivable and the total ratio ensures having enough vertical speed for jumping with both legs connected. The hydrostatic transmission is filled using a high-flow diaphragm pump through multiple manual valves located along the circuits to simplify the filling procedure and minimize the trapped air.

4) *Sharing Unit*: A combination of two motorized three-way L-port ball valves enables to share the same actuator for the left and right knees. Solenoid valves would be faster but are heavy and restrict the flow. The leak-free design and high flow coefficient of ball valves make them suitable for reconfigurable hydrostatics but motorized industrial ball valves are too slow for most robotic devices. The prototype uses a high-speed servomotor designed for RC helicopter tail rotors. An additional 3D printed spur gear multiplier 1 : 2 ($R_{valve} = 0.5$) increases the switching speed. Fig. 8 (left-bottom corner) shows the design. The mass of a valve unit is 247 g (valve 95 g, servomotor 79 g, plastic gears and frame and bolts 73 g). A full switch (180° stroke) takes 80 ms but the output becomes partially connected within 60 ms, at 113°. A more custom valve design could improve the performance. For instance, for leg switching, [19] designed recently a rotary-cage valve with a 24 ms rise time, consumes only 0.1 J/switch and weight 280 g but it is rated for low pressures.

5) *Software and Electronics Implementation*: The controllers were implemented on a Teensy 4.1 running at a steady low-level 1000 Hz rate. Data acquisition is done at a 200 Hz rate on a Jetson Nano. A Maxon 70/10 drives the main motor with a current feedback loop and an Odrive 3.6 drives the motor of the pump with a speed feedback loop. The valves' positions are monitored with CUI AMT103 encoders instead of the internal potentiometer of the servomotors for higher precision.

B. Force Control

The force controller used for the experimental validation is shown in Fig. 10. The goal is to track force trajectories at the output to assist the user movement and reduce its apparent bore payload. The controller converts the total desired normalized GRF forces at the legs ($f_{1,d}$ and $f_{2,d}$) and a static desired force $f_{stat,d}$ into a motor current command $I_{M,cmd}$, a velocity command at the pump $\omega_{p,cmd}$ and an angle command $\theta_{a,cmd}$ at the accumulator valve to stop the pump when the static pressure is reached. For each task, f_{stat} is computed offline

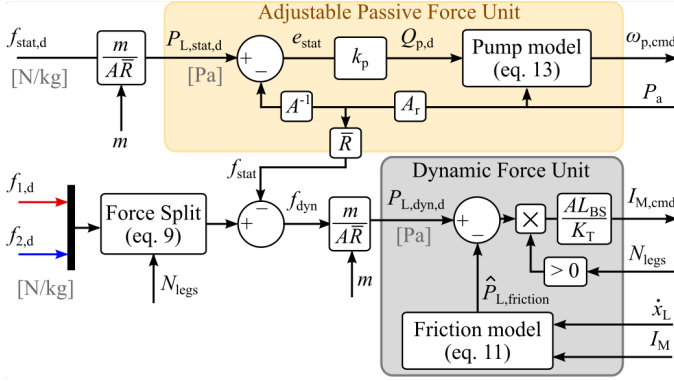


Fig. 10. Force control law for sharing the reference forces between the main motor (EM) and the pump-accumulator unit. Most parameters are defined in Table III or otherwise described in the text.

as in section III (Design D) to minimize the burden and heat losses at the dynamic force unit. Otherwise, it could be solved in real time $f_{static,d}$ to maximize efficiency. The desired forces $f_{1,d}$, $f_{2,d}$ and f_{stat} are converted into desired pressures at the leader piston, after being scaled by the payload mass m and the number of legs connected to the actuation, N_{legs} .

1) *Dynamic Force Unit Controller*: An open-loop controller tracks the desired dynamic pressure $P_{dyn,d}$. In turns, the motor helps track sudden variations of the desired static pressure (e.g., payload m varies rapidly) until $P_{L,stat,d}$ is reached by the pump. Finally, force tracking is improved by using a smoothed Coulomb-viscous friction model:

$$\hat{P}_{friction} = \underbrace{\left(\mu_{seal} + (1 - \eta_{BS}) \left| \frac{I_M K_T}{L_{BS} A_r} \right| \right)}_{\text{Coulomb seal + ballscrew}} \tanh(\gamma \dot{x}_L) + \underbrace{b \dot{x}_L}_{\text{damping}} \quad (11)$$

For stable friction compensation, the friction parameters used are $\mu_{seal} = 0.07$, $\eta_{BS} = 0.96$ and $b = 0.004$. The slope γ is tuned experimentally to 0.3. Fig. 11 shows the force tracking performance when the system is backdriven at 1 Hz.

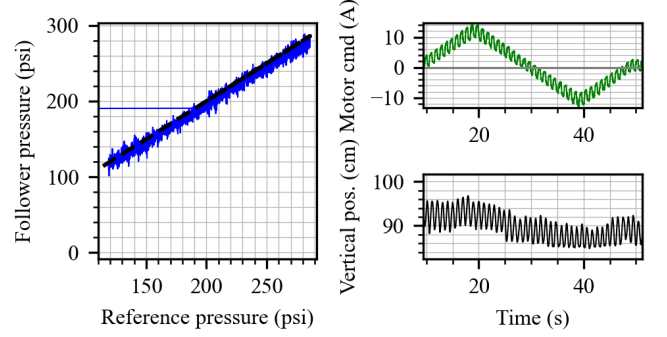


Fig. 11. Force tracking with friction compensation. The system is backdriven vertically at ≈ 1 Hz while an up-down reference force ramp is sent.

2) *Passive Force Unit Controller*: A pressure feedback controller compares the measured accumulator pressure P_a to the desired leader static pressure $P_{L,stat,d}$. The gain $k_p = 2.5$ converts this error into a desired gear pump flow $Q_{p,d}$. To find the required motor velocity command, the pump flow is given in a simplified form as [31]:

$$Q_p = V_{displ.} \omega_p - \underbrace{(\alpha \Delta P_p - \beta \omega_p)}_{Q_{leak}} \quad (12)$$

$V_{displ.}$ being the volumetric displacement. The axial and radial leak flows through the gears Q_{leak} increase with the pump pressure ΔP_p and decreases with the pump velocity ω_p . α and β depend on the geometry and the viscosity of the fluid. From equation 12, the pump control law becomes:

$$\omega_{p,cmd} = \underbrace{\left(\frac{1}{V_{displ.} - \beta} \right)}_{m_Q} Q_{p,d} + \underbrace{\left(\frac{\alpha}{V_{displ.} - \beta} \right)}_{1/m_P} P_a \quad (13)$$

where the coefficients $m_p \approx 9709$ Pa s and $m_Q \approx 9.5$ rad s $^{-1}$ mL $^{-1}$ were found experimentally. Finally, a state machine commands the accumulator valve to stop pumping when the static pressure is reached.

C. Switching Control

Leg switching consists of generating position commands at the servomotors of the valves to switch from the tank position ($\phi_{tank}=0^\circ$) when the force reference is zero, to the leader piston position ($\phi_L=180^\circ$), when $f_1 > 0$ and/or $f_2 > 0$. The internal position feedback controller of the servomotors tracks this reference position. As shown by Fig. 8, the valves can be also be in blocked or partially blocked states, allowing energy dissipation. This is tested in section VII for smoother switching.

The proof-of-concept and controllers are used in the next section to verify the experimental feasibility and efficiency of the proposed concept for multifunctional exoskeletons.

VI. EXPERIMENTAL VALIDATION

This section presents preliminary experimental tests suggesting that the proposed actuator is feasible and can track

a variety of vertical GRF profiles tasks for lower-limb exoskeletons. Some undesired effects are found and discussed, such as relative to leg switching. Also, an energy consumption test is conducted and suggests that the proposed actuator can consume up to 6.3x times less energy for walking. The exoskeleton is not worn by a user here and is guided along a vertical rail. The demonstrations were filmed and presented in the video attached to the paper. Table IV contains all the parameters and references used for the tests.

TABLE IV
PARAMETERS AND REFERENCES USED FOR THE VALIDATION TESTS

Task	Knee ratio	Beared Mass	Right leg	Left leg	Static offset	
	\bar{R}	m	$f_{1,d}$	$f_{2,d}$	$f_{stat,d}$	
		[kg]	[N kg ⁻¹]	[N kg ⁻¹]	[N kg ⁻¹]	
Squatting	0.18	$m_{proto} + m_{load}$	$g/2$	$g/2$	$g/2$	
Jumping	0.18	m_{proto}	charge	0	0	24
			launch in air	24	24	
			land	0	0	
Walking	0.18	m_{proto}	Fig. 4	Fig. 4	8.2**	
Running (60% assist.)	0.18	0	Fig. 4 (60%)	Fig. 4 (60%)	8.5**	
Walking (energy test)	0.34	m_{proto}	Fig. 4	Fig. 4	8.2**	

*Leading to a max pressure reference in the transmission (3.45 MPa).

**Optimal values computed in section III

A. In-Phase Tasks Force Tracking (Combined Legs)

In-phase tasks are tasks where both legs work together and have a similar force profile. Here are validated squatting (or similarly sit-to-stands) and jumping.

1) *Squatting and Adjusting to Varying Payloads*: This test validates that the system and controller can balance gravity force and even automatically adapts to a varying payload (m_{load}) plus the weight of the vertically guided prototype. The exoskeleton is also manually backdriven up and down to simulate a squat-like motion. Fig. 12 shows that the system can automatically pressurize the accumulator to passively balance a measured load. In parallel, the dynamic force controller meets three functions: 1) tracking instant variations of the payload until the accumulator is filled (at 16 s, 36 s and 50 s), 2) canceling out pressure variations ΔP_a due to the volume variations in the accumulator ΔV_a induced by the leader piston being backdriven back-and-forth (at 24 s, 38 s and 54 s), and 3) compensating friction.

2) *High Power Jumping*: Most high force exoskeletons hinder powerful dynamic movements such as jumping because they lack mechanical transparency, have limited actuator speed and have too heavy collocated weight along the legs. The proposed actuator can generate high power using the passive force unit. The jumping sequence is: 1) charge the accumulator while being crouched with the leader piston fully retracted, 2) acceleration until the standing position is reached (< 110 cm), 3) aerial phase (when > 110 cm) where the exoskeleton must not constraint the user's natural movements, 4) land (when < 110 cm). Fig. 13 shows a 33 cm jumping height reached,

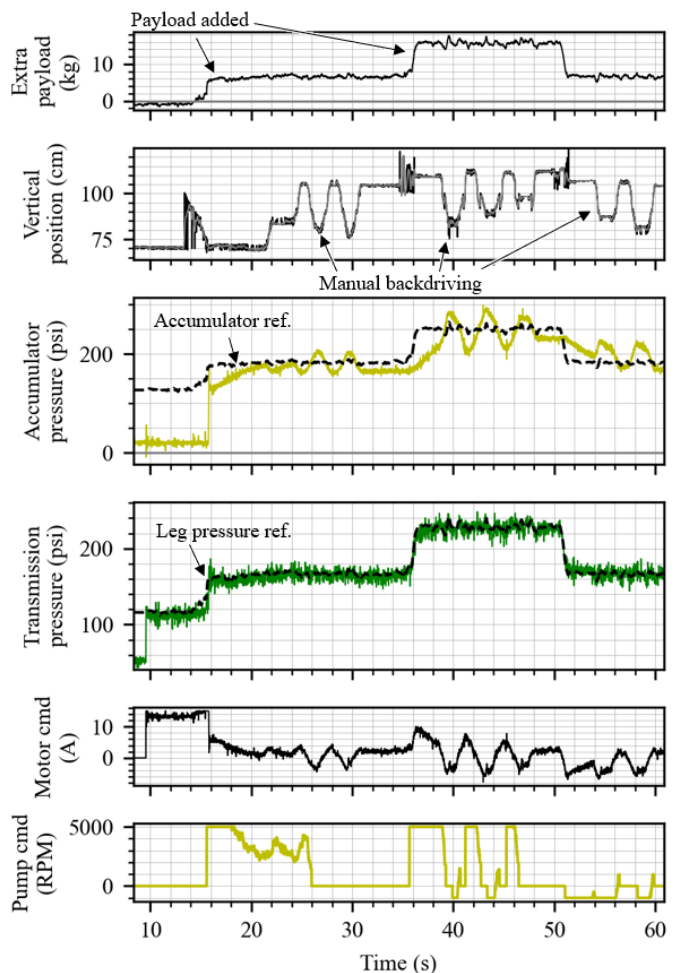


Fig. 12. Squats with varying payload validation. Pressure references in black, pump-accumulator signals in yellow, leader cylinder and motor signals in green, right leg signal in blue and left leg signal in red.

which is near the mean human jumping height. The maximum vertical speed is 3.15 m/s and is near the maximal speed of the motor. During launching, the maximum pressure is not maintained because the dynamic force unit, even at peak torque, cannot overcome the accumulator pressure drop. Then, the valves are fast enough to disconnect the legs from the dynamic and static force units for 88% of the aerial phase. Regarding power, we find during the launching sequence that the average and peak total leg powers are 790 W and 1220 W, respectively (using the slave pressure and the vertical speed signals), while the average and peak powers from the main motor are only 337 W and 507 W (using the motor current and the leader piston speed). These results suggest that the proposed topology extends the force and power capabilities of a low-force lightly geared motor, potentially allowing a user to generate high power and jumps naturally without being hindered. For a maximum power assistance, though, there is a delay before jumping to fill the accumulator completely.

B. Out-of-Phase Tasks Force Tracking (Alternating Legs)

Out-of-phase tasks are when the legs support the load alternatively like for walking and running. These are more

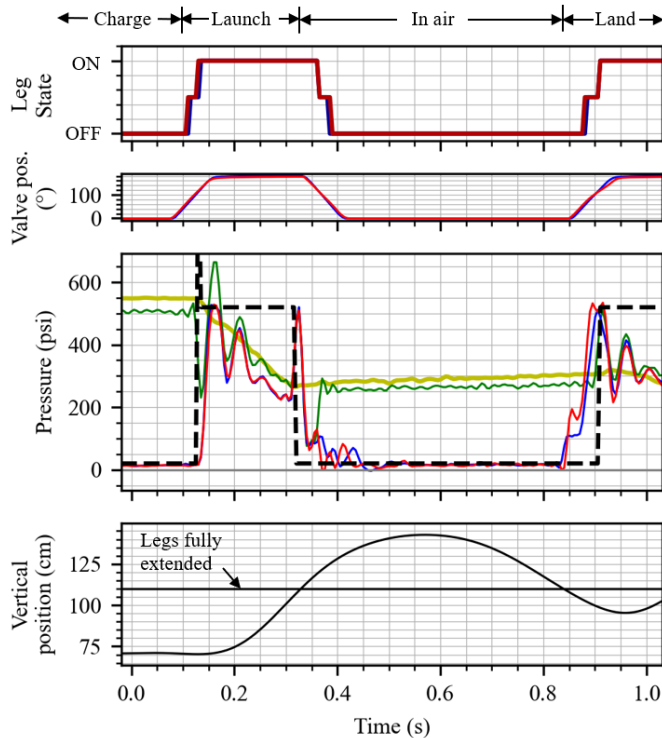


Fig. 13. Jumping validation. Pressure reference in dashed black, accumulator in yellow, leader cylinder in green, right leg in blue and left leg in red.

challenging because the hydrostatic topology is actively re-configured which is discussed in this section.

1) *Walking and Running Force Tracking*: For walking at 1.8 m s^{-1} and running at 4.5 m s^{-1} , the references are the ground reaction force profiles of the first column of Fig. 4 since it corresponds to the output force to generate by each leg. For walking, the exoskeleton is standing and carries its own weight. For running, it is in blocked position since the prototyped actuator cannot generate enough force to jump on one leg. It provides here a 60% running force assistance. The results are given in figures 14 and 15. For walking, the resulting exoskeleton motion is mostly a sine wave, like the actual motion of the center of mass of a human walking. The tests show that the right and left force profiles can be tracked alternatively, even for fast dynamic tasks like running. They also highlight a few limitations and challenges that are discussed next.

2) *Stroke Loss*: For walking, some leader piston stroke is lost every step (here, 0.75 mm/step). This potential elastic energy is lost in the tank when a leg still under pressure gets disconnected which happens during the double support phase of walking. To avoid this, we shall not connect both legs simultaneously during walking, e.g., by prioritizing the assistance of the leading leg only, just like existing walking underactuated exoskeletons do [10], [19]. Surprisingly, stroke losses also happened for the running test but not as much (0.20 mm/step). This is for the same reason: the hydrostatic transmissions were still slightly pressurized when legs got disconnected, probably here due to wrong valve timing. Proper valve timing is thus essential. A pressure condition could be

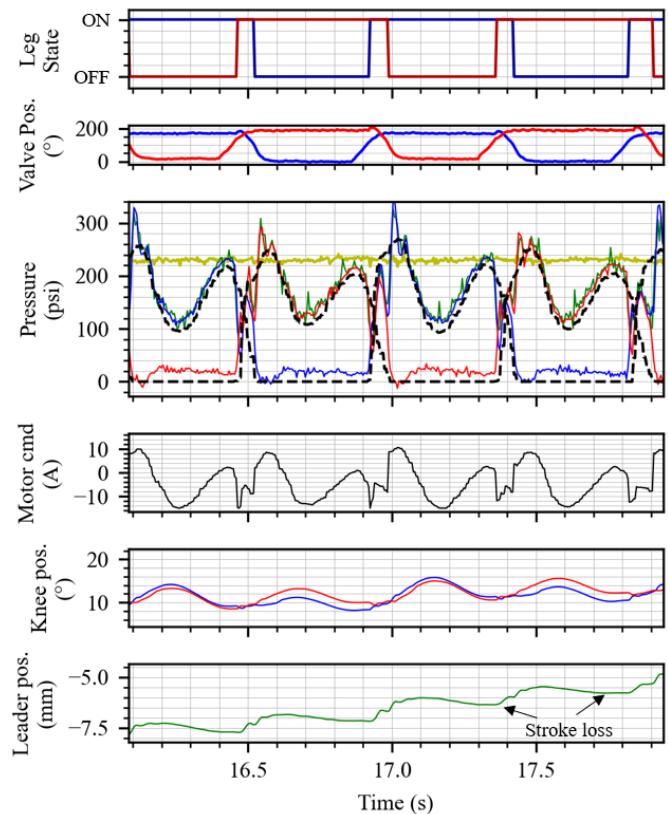


Fig. 14. Walking validation (1.8 m/s force profile) with the exoskeleton self-standing and free to move. Pressure reference in dashed black, accumulator in yellow, leader cylinder in green, right leg in blue and left leg in red.

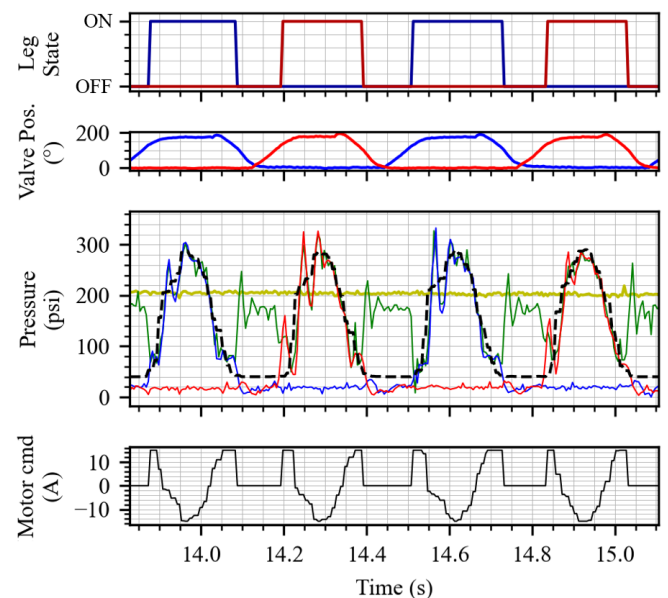


Fig. 15. Running force tracking validation (4.5 m/s force profile) with the exoskeleton legs blocked. Pressure reference in dashed black, accumulator in yellow, leader cylinder in green, right leg in blue and left leg in red.

added to the valve control law to ensure the pressure is released before switching. Another mitigation to prevent missing stroke could be 1) replacing the leader piston by a hydraulic actuator with unlimited stroke, like a novel backdrivable and efficient

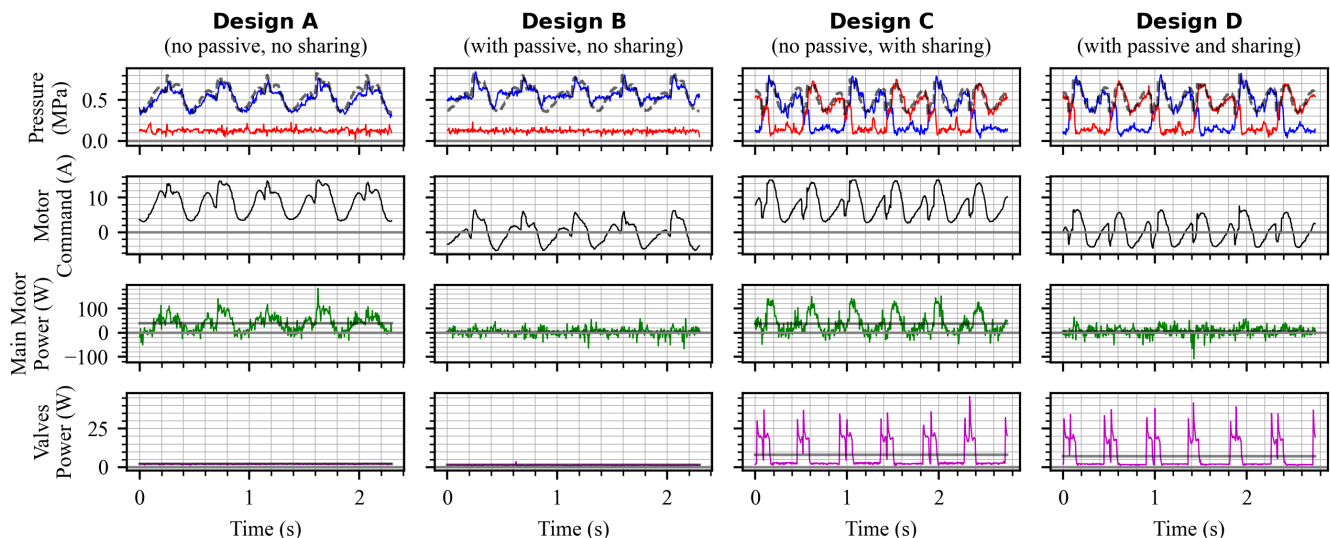


Fig. 16. Energy consumption tests for Designs A–D when tracking the vertical GRF of walking. To imitate Designs A and B (one motor per leg), the single motor tracks the total GRF of both legs with the right leg only.

pump, or 2) modify the actuator topology so that the pump can refill the hydrostatic transmission when needed.

3) *High Frequency Pressure Oscillations*: For running and walking, oscillations that match the transmission natural frequency occur when the legs get connected and when the main motor commands vary instantly, i.e., when N_{legs} changes discretely between 1 and 2 in equation 9. It is not clear if these oscillations would be perceptible to a user, though. Model-based control laws for hydrostatic transmissions may be used to minimize overshoots and keep a high control bandwidth [32]. The oscillations due to valve switching could also be mitigated by dissipating energy actively with the valves which is explored in section VII.

4) *Valve Switching Delay*: For walking and running, the valves were switched ≈ 65 ms in advance so that the legs get connected at the right time. For a realistic use-case scenario, we would need to estimate the percentage of the gait cycle in real time to synchronize leg connections. Moreover, the tests do not show if the swinging leg would be hindered by the valve momentarily blocking the transmission during switching. Indeed, if the valves are too slow or the transmissions very stiff, the user may feel resistance if he compresses the transmission during switching. This is addressed in section VII. Though, if the user pulls on the transmission while switching, he would not feel resistance because hydrostatic transmissions cannot transmit tensile forces.

Despite these challenges, the force tracking of vertical GRF of walking and running is feasible. Next is compared the experimental energy consumption of the proposed concept over a simulated fully actuated one to verify the efficiency advantage.

C. Energy Consumption Comparison for Walking

This test compares the experimental energy consumption of Designs A–D in the case of assisting the stance phase of

walking at 1.8 m/s. Therefore, the potential efficiency benefit calculated in section III when adding passive and sharing force units is verified. As is, the main motor of the prototype is, however, not able to lift the whole prototype on one leg without the passive force unit, which is necessary to simulate Designs A and C. Then, the knee ratio is increased here to $\bar{R} = 0.34$ by changing the configuration of the knee transmission (moving the attachment point of the follower cylinders). The accumulator precharge pressure is changed to 0.48 MPa as well. For testing Designs A and C (no passive force unit), the accumulator is disconnected using its dedicated valve. To reproduce Designs A and B, all the GRF references ($f_{1,d} + f_{2,d}$) are sent to the right leg only because the prototype just have a single motor. The results are given in Fig. 16. The average power consumption from the main motor for Designs A–D are 38.5 W, 3.2 W, 36.2 W and 6.1 W, respectively. Compared to Design A (baseline), Design B consumes 12x less, Design C consumes 1.1x less and Design D consumes 6.3x less. This confirms the results from Table I which neglected the consumption of the valves and the transmission losses. By comparison, the hydrostatic static force unit in [19] reduced the energy consumption of walking by 65% (including swing phase). Also, the mean valves' consumption is ≈ 7 W, or ≈ 3.5 J each time both legs are switched, which is relatively small compared to the power consumed by Design A. Still, a custom design as in [19] could reduce significantly this power consumption and increase the switching speed. All in all, these experiments validate that the proposed actuation is more efficient.

In conclusion, it is reasonable to think that the proposed actuation technology is feasible, multifunctional and more efficient. Careful attention is needed for underactuation during the double support phase of walking to prevent missing stroke. Pressure oscillations and momentarily blocking valves issues are addressed in section VII.

VII. CHALLENGES MITIGATION USING THE VALVES

Many exoskeleton assisting devices that feature discrete transmission modes (e.g., two-speed gear transmissions, clutchable springs, etc.) introduce delays and parasitic effects that can be felt by the user when switching. Parasitic pressure transients were found in Section VI when switching. This section presents deeper insights regarding these effects. We find that both the valve switching speed and the motion of the output while switching have an effect on pressure overshoot. Improvement strategies are tested.

1) *Valve Switching Speed*: When the hydrostatic transmission is suddenly connected to a pressurized actuator, the pressure inside the line overshoots before stabilizing. Pressure feedback could hardly be used to dampen these oscillations with the main motor since it matches the natural frequency of the transmission. Here the effect of valve switching speed is assessed for the case of a static output. The right leg is blocked and the leader piston is pressurized at 1.5 MPa by the accumulator. The right valve is then switched. This procedure is repeated for ten different valve speed values ranging from 2600°s^{-1} (max speed) to 180°s^{-1} . The results in Fig. 17a show that switching slower can help dampen the second order dynamics of the transmission, but at the compromise of longer switching times. This is due to the partially blocked position

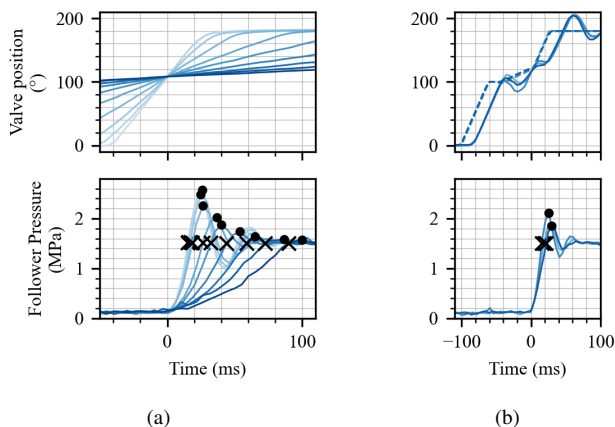


Fig. 17. Effect of the valve speed when connecting the right leg (blocked output) to the leader piston under pressure: a) at fixed switching speeds, b) at variable switching speeds. All tests were synchronized in post-processing where the pressure begins to rise. The dots are the peak values and the crosses give the 0-100% rising time.

of the valve (see Fig. 8) where the head loss through the valve is high. Most hydraulic valves have a similar middle position with high head loss.

The motorized valve can be seen as an extra force input to the dynamic system to dissipate energy on purpose. We propose to vary the valve speed during switching, as demonstrated in Fig. 17b. The valve speed is maximal for most times but is greatly reduced when the valve position is near its partially blocked state. The compromise between switching speed and pressure overshoot is then reduced.

2) *Switching with a Moving Output*: When switching, the valves are blocked for a few milliseconds (see Fig. 8). Meanwhile, the leg becomes passive and the output force is driven by the motion of the output and the stiffness of the hydrostatic

transmission. This could hinder the user at the transitions of tasks as when landing a jump or between the swing and stance phases of walking/running. The tests of Fig. 18 illustrate this effect. The weight of the vertical cart is first balanced by the accumulator. Then, the cart is manually moved in one direction and leg switching is triggered when a given vertical speed condition is met (upward and downward motions at 0.25 m/s, 0.5 m/s and 1.0 m/s). The valves switch at maximum speed. A series of tests were also conducted for a slower switching speed (200 ms) but are not presented here for conciseness. On one hand, switching while the output is moving upward

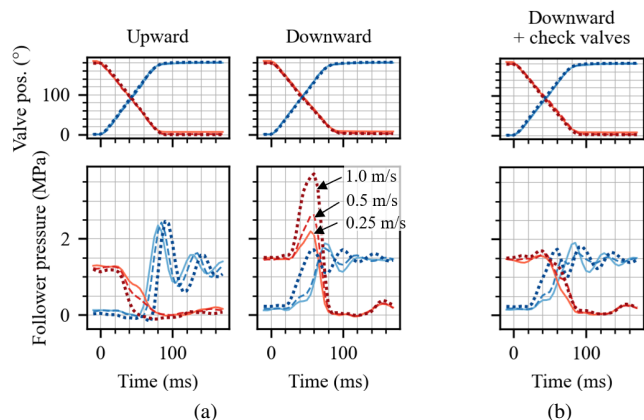


Fig. 18. Leg switching tests at different output cart velocities (0.25 m/s = solid lines), 0.50 m/s = dashed lines and 1.00 m/s = dotted lines): a) when the output is moving upward and downward, b) solution for improving the downward switch using check valves to by-pass the flow. Blue and red lines are for the right and the left leg measurements, respectively.

has minor effects on the user. Indeed, the line depressurizes in advance, down to ≈ 0 MPa (vacuum), removing the force applied to the output/user but not restricting its motion. On the other hand, when switching during a downward motion, the valve restricts the motion of the output/user. Actually, the faster the output is moving and the slower the valves are (and the stiffer the transmission is), the higher the pressure overshoot is. To mitigate this effect, we propose to add two optional check valves in parallel to the leg valves (see Fig. 8) to by-pass them when they are in the blocked position. Check valves are typically small and inexpensive components. As expected and shown by Fig. 18b, this removes the overshoot when the output is moving downward. A beneficial side effect is also that the leg gets connected faster through the check valves, independently of the valve switching speed performance.

VIII. DISCUSSION AND CONCLUSION

Fully actuated robots using lightly geared motors are truly multifunctional but are inefficient and requires heavy motorization. Quasi-passive and underactuated robots are more efficient and use less motors, respectively, but at the expense of typically being task specific. This paper presented a new reconfigurable hydrostatic concept that combines a static load compensation and a sharing mechanism by leveraging the use of hydrostatic transmissions. It can assist both in-phase (squats, jumps) and out-of-phase (walk, run) tasks and the passive assistance can be adjusted in real time for a varying

payload or bodyweight assistance. This hybrid concept is thus multifunctional.

For the specific case of a load-bearing exoskeleton, analytical calculations highlighted the potential benefits of a static force unit and a sharing unit on relaxing the motorization requirements and improving efficiency. A case study design with off-the-shelf components clarified that the proposed concept, even if more complex, can have a similar actuation weight while being more backdrivable and efficient. However, for a weak exoskeleton case study, the mass overhead due to the extra components of the proposed design could be heavier than the saved mass on motorization. Also, despite the advantage of delocalized actuation, the use of hydrostatic transmissions can have a significant impact on the total mass. Engineering efforts for more force-dense miniature hydraulic actuators would help in that sense. All in all, the proposed concept becomes more and more relevant as the force and autonomy requirements of a load-bearing exoskeleton increase. Finally, the experimental validations showed that the proposed reconfigurable hydrostatic design works for tracking the vertical GRF of various tasks. The energy consumption advantage was also confirmed for walking. With the sharing unit, special attention is advised though for potential missing stroke issues, especially if for assisting the double support phase of walking. Moreover, the tests showed that leg switching is possible using relatively slow valves, as long as it is acceptable to begin switching in advance by estimating the gait cycle.

Future tests are needed to finalize the validation with a user wearing the exoskeleton and executing the swing phases, ensuring that switching feels comfortable. Still, promising mitigation using valves were suggested and tested to reduce the switching effects that could be felt by the user. An embedded and optimized actuator prototype should be developed as well to ensure its competitiveness versus classical actuation approaches. Finally, this work could be extended to load-bearing legged robots (without the sharing unit), using one centralized adjustable static force unit for all the legs.

REFERENCES

- [1] S. Seok, A. Wang, M. Y. Chuah, D. J. Hyun, J. Lee, D. M. Otten, J. H. Lang, and S. Kim, "Design Principles for Energy-Efficient Legged Locomotion and Implementation on the MIT Cheetah Robot," *IEEE/ASME Transactions on Mechatronics*, vol. 20, no. 3, pp. 1117–1129, Jun. 2015. [Online]. Available: <https://ieeexplore.ieee.org/document/6880316/>
- [2] A. SaLoutos, E. Stanger-Jones, Y. Ding, M. Chignoli, and S. Kim, "Design and Development of the MIT Humanoid: A Dynamic and Robust Research Platform," in *2023 IEEE-RAS 22nd International Conference on Humanoid Robots (Humanoids)*, Dec. 2023, pp. 1–8, iSSN: 2164-0580. [Online]. Available: <https://ieeexplore.ieee.org/document/10375199?arnumber=10375199>
- [3] T. Elery, S. Rezazadeh, C. Nesler, and R. D. Gregg, "Design and Validation of a Powered Knee–Ankle Prosthesis With High-Torque, Low-Impedance Actuators," *IEEE Transactions on Robotics*, vol. 36, no. 6, pp. 1649–1668, Dec. 2020, conference Name: IEEE Transactions on Robotics.
- [4] N. Kashiri, A. Abate, S. J. Abram, A. Albu-Schaffer, P. J. Clary, M. Daley, S. Faraji, R. Furnemont, M. Garabini, H. Geyer, A. M. Grabowski, J. Hurst, J. Malzahn, G. Mathijssen, D. Remy, W. Roozing, M. Shahbazi, S. N. Simha, J.-B. Song, N. Smit-Anseeuw, S. Stramigioli, B. Vanderborght, Y. Yesilevskiy, and N. Tsagarakis, "An Overview on Principles for Energy Efficient Robot Locomotion," *Frontiers in Robotics and AI*, vol. 5, Dec. 2018, publisher: Frontiers. [Online]. Available: <https://www.frontiersin.org/journals/robotics-and-ai/articles/10.3389/frobt.2018.00129/full>
- [5] C. Khazoom, C. Véronneau, J.-P. L. Bigué, J. Grenier, A. Girard, and J.-S. Plante, "Design and Control of a Multifunctional Ankle Exoskeleton Powered by Magnetorheological Actuators to Assist Walking, Jumping, and Landing," *IEEE Robotics and Automation Letters*, vol. 4, no. 3, pp. 3083–3090, Jul. 2019.
- [6] M. Grimmer, M. Eslamy, S. Glied, and A. Seyfarth, "A comparison of parallel- and series elastic elements in an actuator for mimicking human ankle joint in walking and running," in *2012 IEEE International Conference on Robotics and Automation*, May 2012, pp. 2463–2470, iSSN: 1050-4729.
- [7] G. Elliott, A. Marecki, and H. M. Herr, "Design of a Clutch–Spring Knee Exoskeleton for Running," *Journal of Medical Devices-transactions of The Asme*, vol. 8, no. 3, p. 031002, Sep. 2014, mAG ID: 2052232537.
- [8] A. M. Dollar and H. Herr, "Design of a quasi-passive knee exoskeleton to assist running," in *2008 IEEE/RSJ International Conference on Intelligent Robots and Systems*, Sep. 2008, pp. 747–754, iSSN: 2153-0866.
- [9] E. Gizzo and E. Ackerman, "Boston Dynamics' Marc Raibert on Next-Gen ATLAS: "A Huge Amount of Work"," 2016. [Online]. Available: <https://spectrum.ieee.org/boston-dynamics-marc-raibert-on-nextgen-atlas>
- [10] A. T. Asbeck, K. Schmidt, I. Galiana, D. Wagner, and C. J. Walsh, "Multi-joint soft exosuit for gait assistance," in *2015 IEEE International Conference on Robotics and Automation (ICRA)*, May 2015, pp. 6197–6204, iSSN: 1050-4729.
- [11] J. Denis, A. Lecavalier, J.-S. Plante, and A. Girard, "Multimodal Hydrostatic Actuators for Wearable Robots: A Preliminary Assessment of Mass-Saving and Energy-Efficiency Opportunities," in *2022 International Conference on Robotics and Automation (ICRA)*. Philadelphia, PA, USA: IEEE, May 2022, pp. 8112–8118. [Online]. Available: <https://ieeexplore.ieee.org/document/9812435/>
- [12] M.-A. Lacasse, G. Lachance, J. Boisclair, J. Ouellet, and C. Gosselin, "On the design of a statically balanced serial robot using remote counterweights," in *2013 IEEE International Conference on Robotics and Automation*, May 2013, pp. 4189–4194, iSSN: 1050-4729. [Online]. Available: <https://ieeexplore.ieee.org/abstract/document/6631169>
- [13] S. K. Banala, S. K. Agrawal, A. Fattah, V. Krishnamoorthy, W.-L. Hsu, J. Scholz, and K. Rudolph, "Gravity-Balancing Leg Orthosis and Its Performance Evaluation," *IEEE Transactions on Robotics*, vol. 22, no. 6, pp. 1228–1239, Dec. 2006, conference Name: IEEE Transactions on Robotics.
- [14] Y. Zhang, J. Jiang, and N. G. Tsagarakis, "A Novel Passive Parallel Elastic Actuation Principle for Load Compensation in Legged Robots," *IEEE Robotics and Automation Letters*, vol. 9, no. 10, pp. 8881–8888, Oct. 2024. [Online]. Available: <https://ieeexplore.ieee.org/document/10643641/>
- [15] S. Y. Kim and D. J. Braun, "Variable Stiffness Floating Spring Leg: Performing Net-Zero Energy Cost Tasks Not Achievable Using Fixed Stiffness Springs," *IEEE Robotics and Automation Letters*, vol. 8, no. 9, pp. 5400–5407, Sep. 2023, conference Name: IEEE Robotics and Automation Letters. [Online]. Available: <https://ieeexplore.ieee.org/document/10173556>
- [16] N. G. Tsagarakis, S. Morfey, H. Dallali, G. A. Medrano-Cerda, and D. G. Caldwell, "An asymmetric compliant antagonistic joint design for high performance mobility," in *2013 IEEE/RSJ International Conference on Intelligent Robots and Systems*. Tokyo: IEEE, Nov. 2013, pp. 5512–5517. [Online]. Available: <http://ieeexplore.ieee.org/document/6697155/>
- [17] W. Roozing, Z. Li, G. A. Medrano-Cerda, D. G. Caldwell, and N. G. Tsagarakis, "Development and Control of a Compliant Asymmetric Antagonistic Actuator for Energy Efficient Mobility," *IEEE/ASME Transactions on Mechatronics*, vol. 21, no. 2, pp. 1080–1091, Apr. 2016. [Online]. Available: <http://ieeexplore.ieee.org/document/7303955/>
- [18] W. Roozing, Z. Ren, and N. G. Tsagarakis, "Design of a Novel 3-DoF Leg with Series and Parallel Compliant Actuation for Energy Efficient Articulated Robots," in *2018 IEEE International Conference on Robotics and Automation (ICRA)*. Brisbane, QLD: IEEE, May 2018, pp. 1–8. [Online]. Available: <https://ieeexplore.ieee.org/document/8460493/>
- [19] W. Fan, Z. Dai, W. Li, and T. Liu, "Load-Carrying Assistance of Articulated Legged Robots Based on Hydrostatic Support," *IEEE Robotics and Automation Letters*, vol. 9, no. 10, pp. 8274–8281, Oct. 2024, conference Name: IEEE Robotics and Automation Letters. [Online]. Available: <https://ieeexplore.ieee.org/document/10629043>
- [20] C. A. Fukuchi, R. K. Fukuchi, and M. Duarte, "A public dataset of overground and treadmill walking kinematics and kinetics in healthy

- individuals,” *PeerJ*, vol. 6, p. e4640, Apr. 2018. [Online]. Available: <https://www.ncbi.nlm.nih.gov/pmc/articles/PMC5922232/>
- [21] R. K. Fukuchi, C. A. Fukuchi, and M. Duarte, “A public dataset of running biomechanics and the effects of running speed on lower extremity kinematics and kinetics,” *PeerJ*, vol. 5, p. e3298, May 2017, publisher: PeerJ Inc. [Online]. Available: <https://peerj.com/articles/3298>
- [22] H. K. Ko, S. W. Lee, D. H. Koo, I. Lee, and D. J. Hyun, “Waist-assistive exoskeleton powered by a singular actuation mechanism for prevention of back-injury,” *Robotics and Autonomous Systems*, vol. 107, pp. 1–9, Sep. 2018. [Online]. Available: <https://linkinghub.elsevier.com/retrieve/pii/S0921889018300794>
- [23] F. Lanotte, A. Baldoni, F. Dell’Agnello, A. Scalamogna, N. Mansi, L. Grazi, B. Chen, S. Crea, and N. Vitiello, “Design and characterization of a multi-joint underactuated low-back exoskeleton for lifting tasks,” in *2020 8th IEEE RAS/EMBS International Conference for Biomedical Robotics and Biomechatronics (BioRob)*. New York City, NY, USA: IEEE, Nov. 2020, pp. 1146–1151. [Online]. Available: <https://ieeexplore.ieee.org/document/9224370/>
- [24] E. Tricomi, N. Lotti, F. Missiroli, X. Zhang, M. Xiloyannis, T. Müller, S. Crea, E. Papp, J. Krzywinski, N. Vitiello, and L. Masia, “Underactuated Soft Hip Exosuit Based on Adaptive Oscillators to Assist Human Locomotion,” *IEEE Robotics and Automation Letters*, vol. 7, no. 2, pp. 936–943, Apr. 2022, conference Name: IEEE Robotics and Automation Letters.
- [25] K. Schmidt, J. E. Duarte, M. Grimmer, A. Sancho-Puchades, H. Wei, C. S. Easthope, and R. Riener, “The Myosuit: Bi-articular Anti-gravity Exosuit That Reduces Hip Extensor Activity in Sitting Transfers,” *Frontiers in Neurobotics*, vol. 11, p. 57, Oct. 2017. [Online]. Available: <http://journal.frontiersin.org/article/10.3389/fnbot.2017.00057/full>
- [26] Mawashi, “UPRISE™ Load-Bearing Exoskeleton.” [Online]. Available: <https://mawashi.ca/en/defence-and-security/uprise/>
- [27] P. Liang, W. H. Kwong, A. Sidarta, C. K. Yap, W. K. Tan, L. S. Lim, P. Y. Chan, C. W. K. Kuah, S. K. Wee, K. Chua, C. Quek, and W. T. Ang, “An Asian-centric human movement database capturing activities of daily living,” *Scientific Data*, vol. 7, no. 1, p. 290, Sep. 2020. [Online]. Available: <https://www.nature.com/articles/s41597-020-00627-7>
- [28] P. Cormie, J. M. McBride, and G. O. McCaulley, “Power-Time, Force-Time, and Velocity-Time Curve Analysis during the Jump Squat: Impact of Load,” *Journal of Applied Biomechanics*, vol. 24, no. 2, pp. 112–120, May 2008. [Online]. Available: <https://journals.humankinetics.com/view/journals/jab/24/2/article-p112.xml>
- [29] Robodrive, “Motor Parameters ILM38x12,” 2021. [Online]. Available: https://www.tq-group.com/filedownloads/files/products/robdribe/extended_data-sheets/drva_db-lim-kits_ilm38x12_rev200.pdf
- [30] J. M. Hollerbach, I. W. Hunter, and J. Ballantyne, “A comparative analysis of actuator technologies for robotics,” Aug. 1992. [Online]. Available: <https://scinapse.io/papers/1554436968>
- [31] Logan T. Williams, “Fundamentals of External Gear Pump Design,” 2022.
- [32] J. Denis, J.-S. Plante, and A. Girard, “Low-Level Force-Control of MR-Hydrostatic Actuators,” *IEEE Robotics and Automation Letters*, pp. 3849–3856, 2021. [Online]. Available: <https://ieeexplore.ieee.org/document/9369880/>